Direct imaging of fluctuations near the critical point of binary liquids[1]

John Hegseth[2], D. Beysens[3], and Y. Garrabos[4]

1 Paper presented at the Fifteenth Symposium on Thermophysical Properties, June 22-27, 2003, Boulder, Colorado, U.S.A.

2 Department of Physics, University of New Orleans, New Orleans LA

3 ESEME, Service des Basses Températures, CEA-Grenoble, F-38054 Grenoble Cedex 9, France.

4 ESEME, Institut de Chimie de la Matière Condensée de Bordeaux, CNRS, Université de Bordeaux I, Avenue du Dr. Schweitzer, F-33608 Pessac Cedex, France.

ABSTRACT

We use a bench top optical microscope with spatially coherent light to directly visualize concentration fluctuations in a binary liquid (methanol and partially deuterated cyclohexane) near its consulate critical point. We study the nature and mechanism of the image formation by applying both a phase-contrast and dark-field filter to our microscope. Although bright field, phase-contrast and dark field images of phase separating domains are markedly different, we find that the phase-contrast image show only slight changes from the bright field image. This result suggests that the fluctuating media is not a phase object but rather an amplitude object. An analysis of the probability distribution functions shows that the tails deviate appreciably from Gaussian statistics.

KEY WORDS: critical point, concentration fluctuation, light scattering, microscopy

1. Introduction

When small changes are made in a system's thermodynamics state variables, a system will respond by minimizing its free energy, $F(T,X)$ where X is a quantity that characterizes a system such as density, magnetization, or concentration. If this potential has two minima, then two phases co-exist. When T is varied, F may split from a potential with one minimum to a potential with two minima and $X(T)$ bifurcates at the point (T_c, X_c) indicating a phase transition. To describe such a phase transition, we define the order parameter, $M=X-X_c$, defined to be $M=0$ in the disordered state (before the bifurcation) and, $M>0$ in the ordered state (after the bifurcation) indicating a microscopic ordering or increase in symmetry. Exactly at the point (T_c, X_c), $[(\partial^2 F/\partial X^2)]_T=0$ and this point is called the critical point. Near the critical point, the potential minimum is quite spread out in M allowing a large range of probable M fluctuations, δM, in the system. The large range of δM's that exist near the critical point is manifested by extremely large or small values of the thermo-physical properties of the system. These extreme values, both equilibrium properties and transport properties, behave according to universal power laws that either diverge to infinity or converge to zero at the critical point. In particular, this singular behavior is widely believed to include spatial domains of M that are statistically self-similar at T_c, the critical temperature. Fluctuations exist at all length scales at the critical point such that the fluctuation-fluctuation correlation length diverges at T_c, $\xi = \xi_0((T/T_c)-1)^{-\nu}$, where ξ_0 and ν are the system dependent correlation amplitude and the universal exponent, υ=0.63.

A unified explanation for these phenomena has been given by the renormalization group theory that takes the Hamiltonian of a system and "evolves" in its parameter space

through repeated "renormalization" transformations. This transformation consists of a re-scaling followed by normalization and is done repeatedly until a "fixed point" is found, i.e. point in parameter space where the transformation leaves the Hamiltonian invariant. Although this theory is fundamental, being used to describe many disparate areas of physics (e.g., high-energy particles and turbulence), the only satisfactory experimental systems that currently exists for testing it are experiments performed near the critical point of a phase transition.

The system discussed below, a binary liquid of methanol and partially deuterated cyclohexane, exhibits critical behavior when the temperature and concentration are near a critical point in *(c, T)* space where *c* is the concentration of one of the chemical species. The binary liquid system is prepared by mixing two chemical substances such that the concentration of one of them is at a well-known critical concentration c_c [1]. The system will mix or separate depending on *T*, as described above and the order parameter of this system is $M=c-c_c$. The increase in the fluctuation correlation size is manifested by an increase near the critical point of the scattered light intensity. When fluctuations in *M* are the size of the wavelength of light, they strongly scatter light, producing a striking visual effect called critical opalescence. This allows the properties of near critical fluids to be probed with light scattering techniques [2] [3].

Direct microscopic observations of fluctuations have previously been reported [4-5] using spatially coherent light and a bright field technique. The image formation was explained by the interference between the scattered light and the transmitted light. In the following, we investigate other possibilities by varying the optical techniques and image processing.

2. Experiments

To reduce possible sedimentation we have used a density matched mixture of methanol and partially deuterated cyclohexane (CC*-Me, with a critical concentration c_c=71% cyclohexane by weight) [1]. Although the CC*-Me allows the density to be precisely matched, when quenched below T_c=46.64^{0}C, sedimentation of the phase separated drops is clearly visible in the microscopic field of view after several hours. This mixture is placed between two 10mm diameter sapphire windows (8.5mm thick) separated by a gold-coated 3mm thick brass spacer. This sample is placed in a larger copper housing of diameter 6 cm and length *6* cm. Although this cell was filled to a slightly off critical concentration $c=(c_c-0.01)\pm0.002$, it is well within the concentration range $|c-c_c|<0.05$ where fluctuations are visible as reported in reference [5].

In order to conveniently use the optical microscopy system, shown in Figure 1, we have designed a thermal control system that uses air convection and radiation for heat transfer. The cell and housing is temperature controlled by placing it near the center of an aluminum cylinder (D=10 cm and L=18 cm) that has a foil heater glued to its exterior. Two holes in the heating cylinder, aligned with the optical axis of the cell, allow light to enter and leave the sample fluid. To prevent convective cooling of the sample cell windows, these holes are close at both ends by optical windows. To provide a constant ambient temperature for the inner cylinder, two more thermal shields made of polystyrene of thickness 7 cm surround the heating cylinder. We placed our thermal shields, heating cylinder, etc, on an optical bench shown schematically in Figure 1. Although our wide band source (a 100W halogen lamp) results in a small coherence time or, equivalently, a longitudinal coherence length of ≈ 1μm, the geometry of our setup

gives us a spatial coherence of ≈ 120μm in the object plane of the microscope. Since our microscopic field of view was ≈ 1.5mm, this corresponds to a spatial coherence over 8% of the field of view, or 46 pixels on the CCD area (see Fig.1a).

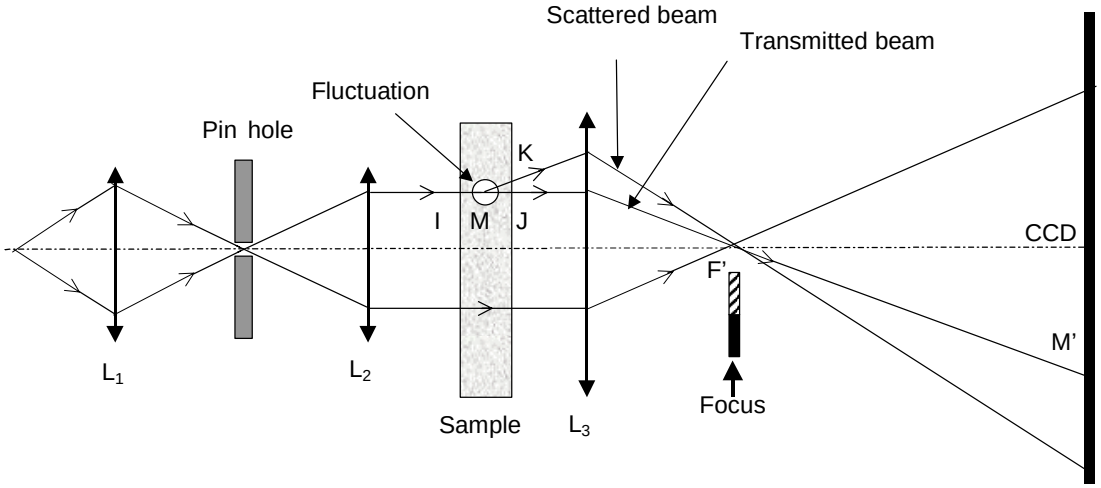

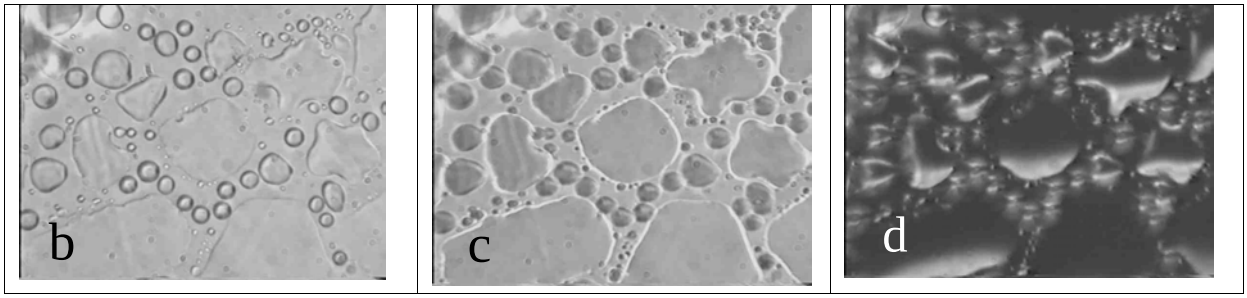

Figure 1. a) In the optical microscopy, a white light source and collimator produced a parallel beam of white light after being focused into a 0.8mm pinhole by 50mm lens. This light is scattered by fluctuations in the turbid media. Magnification is provided by a high quality 50mm photographic lens (Olympus, OM) of numerical aperture 1.2. PC and DF images are produced by sliding a ¼ wave plate and an opaque object to the focus. b), c), and d) shows the BF, PC and DF microscopic images. The hardly visible droplets in the BF image are made visible in the PC image by an optical phase change in the ¼ wave

plate. PC also clearly increases the contrast at very small scales such as the droplet interface and many small droplets. DF produces the same object but with a completely different intensity distribution over the droplet, as is also the usual case for DF images. In our particular case, we note that the phase changes result in droplet images half dark and half bright due to a slightly off center opaque disk.

The sample cell is placed near the focal point of L_3 and its position is adjusted with a translation stage so that the field of view is near the output window of the cell. This is where the contrast is maximized. This also allows a properly positioned object to form an image on a CCD camera (Sony XC-75CE with 752x582 pixels) 1m from L_3. The optical resolution in the object plane is of order of 1 μm, corresponds to both the diffraction resolution ≈ 0.5 μm and the pixel resolution ≈ 0.5 μm. We know from the theory of Fourier optics [6], that the intensity distribution in the focal plane of a simple lens is the Fourier transform of the object. In our experiment, we have performed several manipulations or filters to the light in this as shown in Figure 1. Images with no filters present in the focal plane of L_3, are called *bright-field* (BF) images [4-5].

The first treatment, that we call *phase contrast* (PC), consisted of passing the light through a mica quarter-wave-plate of 1cm diameter. This corresponds to 4% of the lens area or an angle of 0.1 radian for output light. The light that passes through this plate are, over the broad band of optical wavelengths, retarded in phase by $\pi/2$ radians relative to what it would have been had it not passed through it. The light that is focused on this plate is primarily that part of the incoming wave field that we call the transmitted light, i.e., the part of the incoming parallel light wave not scattered by an index of refraction fluctuation. The light that does not pass through this plate is scattered by a fluctuation and

is not rotated. An object that changes only the phase and not the amplitude of the light (e.g., no energy absorption) would produce no net intensity change at the detector, because the phase cancels when the magnitude of the wave is taken at the detector. By rotating the transmitted light at the lens's output focal plane, the wave at the detector is decomposed into two parts that interact making phase objects visible by converting a phase variation into an intensity variation (see Figure 1c).

The second treatment, that we call *dark-field* (DF), used a 7mm diameter opaque disk, placed at the output focal point of L_3, to block the transmitted beam and only allow the scattered light to enter the CCD array. Both of these elements were positioned at the focal plane using the same support. The plane of this support was positioned perpendicular to the optical axis and connected to another translation stage. This stage allowed the support to be displaced perpendicular to the optical axis such that i) the light would pass through the focus unaltered (BF), ii) the light near the focus passed through the quarter-wave-plate (PC), and iii) light was blocked at the focus by the opaque disk (DF). This allowed the three optical techniques to be changed in-situ by adjusting the translation stage (see Figure 1).

Because our method of separating the scattered and transmitted light in the binary liquid set-up is not the same that is normally used in commercial microscopes we first tested our system with images of phase separated droplets. This produces circumstances where PC and DF are normally effective so that we could verify that our PC and DF systems worked. Figure 1b-d shows images of phase separated methanol droplets using the three optical techniques. PC clearly increases the contrast of the droplet interface, as is the usual case for PC images. We can also see how the optical phase change between

the liquid and the gas that is not visible in the BF image is converted into an intensity change in the PC image. DF produces the same object but with a completely different intensity distribution over the droplet, as is also the usual case for DF images [6].

The cell was first heated above T_C (to approximately 50^0C) where the binary fluid was thoroughly mixed and allowed to sit for at least 12 hours. The temperature was then decreased toward the critical point in steps or temperature quenches. These quenches, ΔT, were decreased in magnitude as T_C was approached with ΔT=1 K far from the critical point and ΔT=1 mK close to the critical point. The PID control could achieve a stability as high as 0.1 mK over 12 hours and was mostly limited by the room temperature fluctuations. Because these quenches often resulted in as much as a 20% undershoot we limited the temperature quenches to 1mK.

Because the phase separation was relatively fast, producing high contrast domains that grow in time, the critical point could be measured to within 0.5mK with the 1mK quenches by observing the image after each quench to see if the fluid separated. The identification of the fluctuations in the images was verified by waiting for over 12 hours at T_c+0.5mK. It was seen that the fluctuations retain the same character and did not phase separate. After each quench, the temperature was allowed to equilibrate for at least 20 minutes before recording the video images of the fluctuations on an HI8 VCR images (European standard).

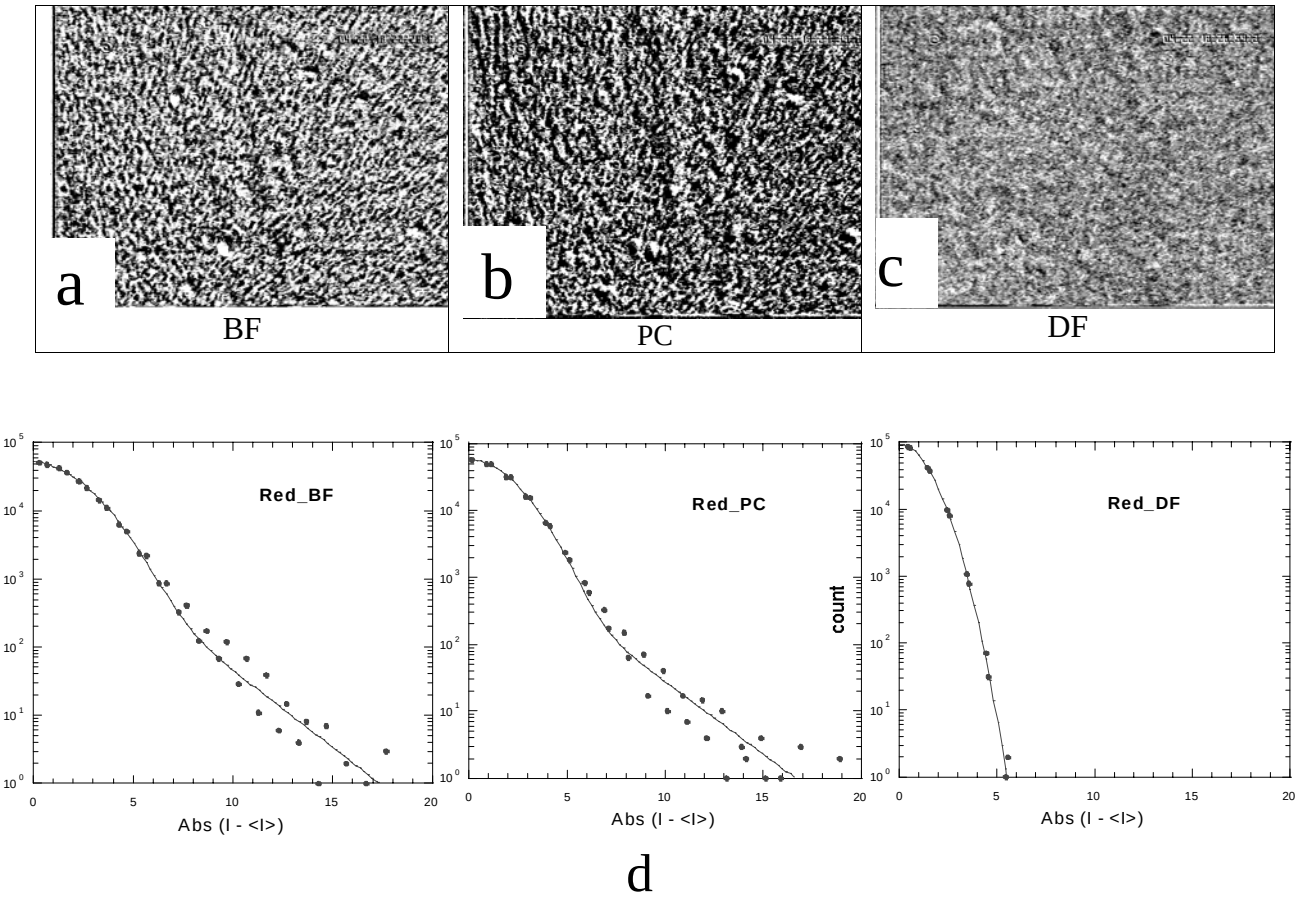

Figure 2. Shown are enhanced a) BF, b) PC, c) DF images taken at ≈ T_c + 1mK (correlation length ξ ≈ 1 μm). Panel d) shows their distributions (histograms) of intensity. These distributions are plotted on a log-lin scale with respect to the absolute value of I - <I> to see the distribution's tail more clearly. The horizontal axis is the intensity scale that is 0 to 255. Our 8-bit black and white digitized images results in 256 possible intensity levels at each pixel and this digitization also limits the number of bins in the histogram. These three intensity histograms have been averaged over 100 histograms at different times to minimize noise error. Optically distorted regions in the image have been excluded in the pixel samples. They have been fitted to the sum of a Gaussian and

an exponential function. The halfwidths of the Gaussians are, BF: 3; PC: 2.6; and DF: 1.6.

We have observed images that exhibit spatial domains of varying light intensity. Figures 2a-c show images taken above and close to the critical temperature, $T_{c,}$ after being processed by the procedure described below. Figure 2d shows the distribution of intensity, or the histogram, that we use to analyze these images. The horizontal axis is the intensity scale that is 0 to 255. Our 8-bit black and white digitized images results in 256 possible intensity levels at each pixel and this digitization also limit the number of bins in the histogram. The spatial sampling of light performed by the CCD camera produces 752x582=437,664 possible pixels to distribute over these 256 intensity values and the vertical axis of the histogram is the number of pixels that contain a given intensity value. The images produced in our system were not of uniform intensity due to system noise from dust, etc. This optical noise gives non-uniform background intensity in addition to the intensity from fluctuations, distorting the intensity histogram. To correct for the optical system noise, we subtracted an image that was time averaged over the one minute of fluctuation time that we collected at a given setting. This insures that the fluctuations in the images do not contribute to background as they average to negligible intensity variations and the noise is constant. Figure 2a shows the BF image, where the average intensity of the treated image has been shifted back to 128 so that it can be displayed. Figure 2b and 2c shows a PC and DF image treated in the same way and taken at the same temperature as the BF image in Figure 2a. In order to eliminate any remaining noisy areas from the image for the histogram, from the time tagging on the video or remaining inhomogeneous regions, these areas were masked out of the histogram so that the

distributions exclude the pixels in these regions. Because these images of the intensity fluctuations are time dependent we could not time average them to minimize random error. Even though the intensity evolves in time the distribution of intensity is stationary, except for random errors that are especially large in the tail of the distribution. We therefore produced time averaged intensity histograms to minimize the system noise and produce a better sample of the distribution tail. The BF, PC, and DF distributions are plotted on a log-lin scale to see the distribution tail more clearly. We also did a similar experiment except that a red filter was applied to the incident light, resulting in increased contrast (the histograms in Fig.2d are calculated from these images). We also recorded the temporal evolution of the fluctuations.

4. Results and Discussion

Intensity variations formed in the BF image were previously explained through an interference mechanism [4-5]. An incident electric field vector, $\boldsymbol{E}$, is decomposed into a transmitted wave, $\boldsymbol{E_T}$, and a wave scattered by the media, $\boldsymbol{E_s}$, that is phase shifted with respect to $\boldsymbol{E_T}$. A fluid element, fluctuating in $\delta M = \delta c$, produces a small change in index of refraction δn ($\delta n \leq 0.01$) in the object volume. This fluctuation produces a phase shift in $\boldsymbol{E_s}$ that is proportional to δn. Because $\boldsymbol{E}$ induces the scattering, $\boldsymbol{E_T}$ and $\boldsymbol{E_s}$ take similar optical paths through the optical system (see Figure 1a), retaining the same phase shift when they coincide in the image plane. Although the incident white light has random polarization, we need only consider one plane of polarization, because the final result is the superposition over all of the equally probable polarization planes. The intensity recorded at a given position in the image plane is, for each polarization component,

$$I = \left|E_T + E_s\right|^2 = E_T^2 + E_s^2 + 2E_s E_T \cos\theta \qquad (1)$$

where $\boldsymbol{E_T}$ is all of the light that is treated by the 1/4 wave-plate (or the opaque disk in DF), $\boldsymbol{E_s}$ is all the light not treated near the output focus, and θ is the phase angle between E_S and E_T . The maximum scattering angle, limited by the aperture of the cell, is 16.7 degrees, giving an effective numerical aperture NA=0.29. $\boldsymbol{E_T}$ is then the superposition of the transmitted light and the light scattered at less then 0.1 radian (angle defined by the PC and DF filters that are approximately the same diameter) and $\boldsymbol{E_s}$ is the superposition of all the light scattered between 0.1 radian and 0.29 radian.

We first note that if the fluctuations only modified the *phase* of the wave, then we would not see any features in BF image. To investigate the extent that a phase modification contributes to the image, we assume that the fluctuation only modifies the phase of the scattered wave, i.e., $\boldsymbol{E_S}$ and then $\boldsymbol{E_T}$ remains constant and any variation in intensity, δI, is due solely to the change in phase produced by the fluctuation. For our case $\cos\theta \approx 1-\frac{1}{2}\theta^2$ so that the measured intensity variation is $\delta I \propto \theta^2$. In PC the ¼ wave plate shifts the phase of E_T by 90°. In this case, according to the above reasoning, $\theta \rightarrow \theta + \frac{1}{2}\pi$ or $\cos\theta \rightarrow \sin\theta \approx \theta$. We thus expect that $\delta I \propto \theta$, producing an image of quite different character. As can be seen in the images in Figures 2a and 2b there is only a small difference between a typical example of these two types of images and no qualitative differences in character.

The intensity distribution of these two images is shown in Figure 2d. We expect $\theta \propto \delta n \propto \delta c$ (concentration fluctuation) so that in a fluctuating thermodynamic system we would expect δc to have a Gaussian distribution. A simple variable substitution, however, implies that the BF image should have an exponential distribution. The BF image, with $\delta I \propto \theta^2$, however, also appears to have a Gaussian distribution in δI. The shapes of these

distributions is thus not consistent with a phase interference mechanism for the formation of the fluctuation image. The temporal evolution of the fluctuations in PC and BF is also very similar. The small differences between BF and PC are probably caused be a slight attenuation of the light from the mica wave-plate that is the slightly opaque, the wave-plate edges, and the mounting piece for the wave-plate.

The DF image in Figure 2c and the intensity distribution shown in Figure 2d reveal differences between DF and BF (or PC) images and the corresponding intensity distribution. In particular, the BF and PC intensity distribution exhibit tails, whereas the DF distribution does not. Because the image of well-identified domains (drops in Fig. 1d) is deeply modified in our set-up, it is difficult to draw conclusions. We note that it was necessary to increase the incident light intensity by a factor of 4.8 to see the DF image.

The fact that the same fluctuating images, with the same intensity distribution, are observed either in BF or PC suggests that very little of the image intensity variations are caused by the interference mechanism. In other words, the image should be the incoherent superposition of the transmitted light ($\boldsymbol{E_T^2}$) and the scattered light ($\boldsymbol{E_S^2}$). In the language of Fourier optics, the optical disturbance produced by the fluctuation is an amplitude object and not a phase object. Since there is no significant energy absorption, the variation in intensity of this amplitude object is caused by light scattering within the geometrical constraints of our optical system, (i.e., a proportion of the scattered light is blocked before arriving at the lens aperture). We note that it has been widely reported in light scattering experiments [2][7] that close to the critical point multiple scattering becomes a significant effect. When the transmitted light decreases to the level where multiple scattering become dominant, however, (e.g., during phase separation where

domains of each phase form) it is no longer possible to observe any domains. The origin of the fluctuation image should therefore be found from single light scattering (e.g. Ornstein-Zernike), such that large-scale fluctuations can be observed.

At the present state of our investigation, it is unclear whether the image intensity is proportional to δM^2 or δM or to a combination of both. We can further analyse the intensity histogram by considering the probability distribution function (pdf) for a concentration fluctuation. Considering T fixed (but not at T_c), the probability, $p(M)dM$, for a small subsystem (e.g., the pixel volume, of order $10\mu m^3$) to have M between M and $M+\delta M$ is given by:

$$p(M)\, dM = A \exp[(\partial^2 F/\partial M^2)_0 \delta M^2 + O(\delta M^3)]\, dM, \qquad (2)$$

where A is a normalization constant and we have expanded F about its minimum. Far from the critical point, the coefficient $[(\partial^2 F/\partial M^2)]_0$ is large so that the pdf (or its histogram) is Gaussian in δM. If $\delta I \propto \delta M^2$, we expect the intensity histogram to be an exponential, that is, a non symmetrical function with respect to <I>. We have found, however, a symmetrical intensity histogram, i.e., a symmetrical exponential–like distribution in the tails of the BF and PC intensity histogram, as shown in Figure 2d. These tails may reflect the expected non-Gaussian character of the larger fluctuations when, closer to T_c, the coefficient $[(\partial^2 F/\partial M^2)]_0$ becomes very small and the other terms in (2) becomes relatively important. It is therefore more likely that $\delta I \propto \delta M$, through an imaging process that remains to be clearly identified. In this respect, we can only conclude that the deviations from Gaussian statistics that we have observed can be interpreted as due to the close vicinity of the critical point, as expected.

The striking similarity of the PC and BF images begs many questions about the mechanism of image formation for critical fluctuations. The investigation of this image formation will require more refined experimental and theoretical studies.

ACKNOWLEDGEMENTS

This work was supported by NASA Grants NAG3-1906 and NAG3-2447. CNES support is acknowledged.

References

1. C. Houessou, P. Guenoun, R. Gastaud, F. Perrot and D. Beysens, Phys. Rev. A **32**, 1818 (1985).

2. D. S. Cannell, Phys. Rev. A **12**, 225 (1975).

3. P. Jany and J. Straub, Int. J. Thermophys. **8**, 165 (1987).

4. P. Debye and R. T. Jacobsen, J. Chem. Phys. **48**, 203 (1968).

5. P. Guenoun, F. Perrot, and D. Beysens, Phys. Rev. Lett. **63**, 1152 (1989).

6. G. Reynolds, J. De Velis, G. Parrent, B. Thompson, *Physical Optics Notebook*, (SPIE, Bellingham, Washington and AIP, New York, 1989).

7. D. Beysens and G. Zalczer, Optics Comm. 26, 172-176 (1978)